SUPPORTING INFORMATION

Atomistic adsorption of PETase onto large-scale PET 3D-models that mimic reality

Paiva, P.[1], Ippoliti, E.[2], Carloni, P.[2,3], Fernandes, P.A. [1], and Ramos, M.J.[1] *

[1] LAQV@REQUIMTE, Departamento de Química e Bioquímica, Faculdade de Ciências, Universidade do Porto, Rua do Campo Alegre s/n, 4169-007, Porto, Portugal *email: mjramos@fc.up.pt

[2] Institute of Advanced Simulations IAS-5/Institute for Neuroscience and Medicine INM-9, Forschungszentrum Jülich GmbH, Wilhelm-Johnen-Straße, Jülich, D-52425, Germany

[3] Physics Department, RWTH Aachen University, Aachen D-52074, Germany

Contents

1. Computational Methods

1.1. cPET models construction, parameterization, and minimization

The cPET models were assembled by replicating the crystalline unit cell of PET in the x, y, and z directions. To do so, the PropPDB program, included in the AmberTools18 package of Amber 2018,[1] was employed. This unit cell, which exhibits a triclinic lattice, was built using Avogadro 1.2.0 software,[2] according to the following parameters determined by Daubeny and Bunn: a = 4.56Å, b = 5.94Å, c = 10.75Å, $\alpha = 98.5°$, $\beta = 118°$, and $\gamma = 112°$.[3]

To allow for a versatile approach to designing PET chains of variable length, three distinct PET units were parameterized: a head-PET, a main-chain PET (the unit to be repeated), and a tail-PET. In this way, one can build a polymer chain containing a specified number of identical main-chain PET monomers (connected to each other) and cap its two ends using the head- and the tail-PET units, which act similarly to the N- and C-terminal ends of an amino acid chain. Both the head- and tail-PET units (*i.e.*, the terminal PET monomers of each chain) were capped with methyl groups to avoid an artificial over-representation of polar end groups, as performed elsewhere.[4] The structures of the three PET units were optimized in vacuum at the HF/6-31G(d) level of theory using the Gaussian 09 software (version D).[5] Atomic charges were derived from a RESP (restrained electrostatic potential) fitting method performed with each optimized structure, using the aforementioned theoretical level to keep consistency with the General Amber Force Field (GAFF).[1, 6] Then, each unit's intramolecular and Lennard–Jones parameters were gathered using the Antechamber tool of Amber 2018, and were later combined with the GAFF.

Whenever required, the cPET polymer was solvated with TIP3P water molecules,[7] organized in a rectangular box whose faces were located at least 12 Å from any atom of PET. Additional sizes and shapes of solvent boxes were also considered, although they did not change the behavior of PET (data not shown). To study the behavior of cPET in vacuum, the molecular crystal was placed in the center of a rectangular box with a dimension of approximately 245 Å x 222 Å x 155 Å. Two distinct cPET models were assembled (cPET1 and cPET2) and their structural features are compiled in Table S13.

The two models were submitted to a multi-step energy minimization procedure, carried out with the Amber 2018 simulation package, to remove eventual tensions and prepare both systems for the subsequent MD simulations. In the first minimization step, all water molecules were minimized (cPET1 only); in the second step, all hydrogen atoms were minimized; in the third step, only the terminal monomers (head- and tail-PET) were minimized; in the final step, the entire system was minimized.

1.2.Molecular Dynamics simulations – PET models

The topology and coordinate files generated by the energy minimization protocol in AMBER for all models were converted into the GROMACS[8, 9] format to enable seamless integration with the available high-performance computing (HPC) resources and to optimize computational efficiency. This conversion was accomplished using ParmEd,[10] a specialized tool designed to automate unit conversions and parameter adjustments. By leveraging ParmEd, the integrity of the original AMBER force field parameters was preserved, ensuring consistency and compatibility across simulation platform.[10] The all-atom simulations were performed with the GROMACS software (version 2021.4),[8, 9] using the Verlet cut-off scheme and a non-bonded cut-off value of 10 Å. Periodic boundary conditions were imposed, and the Particle Mesh Ewald scheme[11] was used to treat non-bonded Coulombic interactions. Long-range dispersion corrections were applied to energy and pressure terms. All bonds involving hydrogen atoms were constrained using the LINCS constraint algorithm,[12] which made it possible to use an integration time step of 2 fs.

In total, over 9 μs of simulation time was performed in the course of this work. All simulations shared the same MD settings that were presented in the previous paragraph. The next subsections will provide further detail on the methodological aspects underlying these MD simulations.

1.2.1. cPET MD simulations

The cPET1 model (*i.e.*, solvated cPET) was simulated at different temperatures to assess the stability of the assembled molecular crystal in water and the behavior of its polymeric chains at temperatures ranging from 30 ºC (near *Is*PETase's optimal temperature[13-15]) to 80 ºC (close to PET's T_g). The details on the MD simulations conducted with cPET are summarized in Table S15. The MD protocol was conducted in three replicas, yielding a total of 300 ns of simulation time per temperature stage. In addition, a 1.52 μs MD run was performed at 80 ºC to follow the overall stability of the cPET1 system in a very long simulation.

The cPET2 model (*i.e.*, cPET in vacuum) was submitted to a three-phase MD protocol, similar to that performed with cPET1, except that in this case the *NVT* ensemble was used in all phases of the simulation (Table S14). Three replicas of this MD protocol were performed at 30 ºC, performing a total of 300 ns of simulation time. An additional 1.52 μs-long *NVT* MD simulation was also performed to assess the behavior of this model over a longer period.

1.2.2. cPET to aPET transformation

To simulate the melting of the cPET polymer, we resorted to the cPET2 model and gradually increased its temperature until it exceeded PET's T_m (≈ 267 ºC) by a considerable margin. The cPET2 model was initially heated from 0 to 30 ºC in a 500 ps-long *NVT* heating phase, followed by a 500 ps-long *NVT* equilibration phase and a subsequent 10 ns-long *NVT* production phase. Then, the last state of the

production simulation was gathered and submitted to a new 500 ps-long *NVT* heating phase, where the temperature of the system was raised linearly by 25 ºC, followed by a 500 ps-long *NVT* equilibration phase and a 10 ns-long *NVT* production phase. Eleven additional rounds of this three-phase protocol were successively conducted to gradually increase the temperature of the cPET2 system up to 330 ºC, by the end of which the cPET2 model had already lost its crystalline arrangement. In all heating phases, all atoms of PET were kept fixed.

The newly generated structure was then placed in the center of a new rectangular box whose faces were located at least 17 Å from any atom of PET (dimensions ≈ 209 Å x 204 Å x 505 Å) and later submitted to an equilibration cycle to further relax the system. This cycle, inspired by the work of Hoffmann *et al.*,[16] comprises a series of brief *NVT* and *NPT* MD stages that span various pressure and temperature ranges and simulate phenomena such as compressions/decompressions and heating/cooling, ultimately leading to a structure with realistic density. The resulting configuration of the equilibration cycle underwent an additional *NPT* simulation stage at 27 ºC for 10 ns (a simplistic version of the modification suggested by Karayiannis *et al.*[17]), allowing further relaxation of the polymer at the conditions similar to those to be simulated later. The parameters for the MD simulations comprising this equilibration cycle are summarized in Table S15. A disordered polymeric structure, which was expected to be reasonably relaxed, was obtained at the end of the equilibration cycle. From that point forward, it was regarded as the aPET model.

1.2.3. Determining aPET model's T_g

To predict the aPET's model T_g, we obtained a relaxed aPET structure at 327 ºC and determined its density. To do so, the aPET model (*i.e.*, the resulting structure of the equilibration cycle presented in Table S15) was heated to 327 ºC for 50 ps in the *NVT* ensemble, and subsequently submitted to an *NPT* production run of 10 ns at the same temperature, after which the density of the system was determined. Then, starting with the final structure and velocities from the production run, the aPET model underwent 14 cycles of temperature cooling-equilibration-production, and a new density value was collected at the end of each cycle. The details on these MD cycles are summarized in Table S16. This procedure was repeated until the temperature achieved -23 ºC, well below PET's T_g. Finally, the calculated density values were plotted against the temperature at which they were collected, and the resulting plot was used for the determination of the T_g value.

1.2.4. aPET MD simulations

The behavior of the generated aPET model was assessed in the presence and absence of solvent molecules. In the first case, the aPET model was solvated with TIP3P water molecules, filling a rectangular box whose faces were located at least 17 Å from any atom of PET (Table S13 for more information on this

model). The solvated model was then submitted to a three-step energy minimization procedure, using the Amber 2018 simulation package, where in the first step all water molecules were minimized, in the second step all hydrogen atoms were minimized, and in the third and final step the entire system was minimized. Upon completion of the minimization protocol, the topology and coordinate files for all models were converted into the GROMACS format using the ParmEd tool, as previously described. The minimized system was then submitted to a set of MD simulations, and the protocol of those simulations is summarized in Table S17. Three replicas of this MD protocol were performed at 30 ºC, making a total of 300 ns of simulation time. In addition to the three replicas, a single 500 ns-long MD run was performed to follow the behavior of this model over a longer simulation period.

The aPET in vacuum model (Table S13 for further details on this model) was submitted to a three-phase MD protocol, as performed with the solvated aPET, except that in this case the *NVT* ensemble was used in all phases of the simulation (Table S17). Again, this procedure was conducted in three replicas, yielding a total simulation time of 300 ns. An additional 500 ns-long *NVT* MD simulation was performed to follow the behavior of this model over a longer period.

1.3. PET-*Is*PETase models construction, parameterization, and minimization

The *Is*PETase structure used in the adsorption studies was gathered from the Protein Data Bank, where it was submitted under the PDB ID 6EQE (0.92 Å resolution).[18] Standard protonation states at pH 7.0 were assigned to all residues according to the results from the empirical pKa predictor PROPKA software (version 3.4).[19] as well as visual inspection of the structure. The exception was Lys253, whose side chain was considered to be neutral, as this residue was deeply buried within the protein. The catalytic His237 was protonated at the δ-nitrogen, according to the most likely network of hydrogen bonds formed with the neighboring residues of the catalytic triad, Ser160 and Asp206. Two important disulfide bonds, between Cys203-Cys239 and Cys273-Cys289, were created.

The PyMOL software[20] was then used to place the treated *Is*PETase enzyme near the surface of either the cPET1 or aPET models. The *Is*PETase structure was manually oriented so that its active site cleft was pointing straight to the surface of PET, to avoid a side-on landing and consequent adsorption, which would be unfavorable for a putative catalytic reaction. Then, the *Is*PETase was manually translocated toward PET until it reached a position approximately 4-5 Å above the surface of the truncated cPET1 or aPET models, mimicking a preadsorbed state. Although relatively short, we believe this distance would still allow *Is*PETase to freely rotate and adjust its orientation/conformation before the adsorption process.

The two models, cPET1-*Is*PETase and aPET-*Is*PETase, were solvated with TIP3P water molecules, filling a rectangular periodic box whose faces were located at least 25 Å from any atom of PET or *Is*PETase. Five Cl^- counterions were added to each system to neutralize their overall charge. The resulting solvated

cPET1-*Is*PETase and aPET-*Is*PETase systems comprised approximately 827,000 and 1,700,000 atoms, respectively. The molecular mechanics parameters for the PET models were gathered from GAFF, while those for the *Is*PETase enzyme were drawn from the ff14SB force field.[21] The two solvated models were submitted to a four-step energy minimization procedure, carried out with the Amber 2018 package. In the first step, all water molecules were minimized; in the second step, all hydrogen atoms were minimized; in the third step, only the terminal monomers of PET (head- and tail-PET) and the *Is*PETase's side chains were minimized; in the fourth and final step, the overall system was minimized.

1.4. Molecular Dynamics simulations – IsPETase adsorption on PET

All MD simulations regarding *Is*PETase's adsorption on PET were run with identical settings as those described previously in the "Molecular Dynamics simulations – PET models" section.

The simulations started with a 500 ps-long *NVT* heating phase, where each PET-*Is*PETase system was heated up to 30 ºC, keeping all non-solvent atoms fixed. Subsequently, a 500 ps-long *NPT* equilibration phase was conducted to relax the density of the two systems. Finally, 500 ns-long production runs were carried out in the *NPT* ensemble at the target temperature. Three replicas were performed, yielding a total simulation time of 1.5 μs for each PET-*Is*PETase system.

1.5. Data collection and analysis

The *gmx trjconv* tool of GROMACS was used to process all generated trajectories.

The RMSd was used to assess the structural stability of PET and of *Is*PETase in all MD simulations. All RMSd values were calculated using GROMACS's *gmx rms* tool by superimposing the target structures with the final structure of the equilibration phase by least squares fitting.

The distribution of the torsion angle O-C-C-O in the EG units of PET was computed using the *gmx angle* tool from GROMACS. A *trans/gauche* ratio could then be determined by dividing the sum of the probabilities of *trans* dihedral angles (180 ± 9°) by the sum of the probabilities of gauche dihedral angles (70 ± 9°).[22] The *trans* content is calculated by dividing the sum of the probabilities of *trans* dihedral angles (180 ± 9°) by the sum of the probabilities of all angles.

The characteristic ratio of PET was analyzed in all MD simulations of aPET that were performed in this study. This ratio, that is a measure of the stiffness of a given polymer, was also used for assessing equilibration of the aPET model throughout the simulation. It was calculated according to the following expression:[23, 24]

$$\text{Characteristic ratio } (C_\infty) = \frac{\langle R^2 \rangle}{M},$$

where $\langle R^2 \rangle$ is the average square end-to-end distance, and M corresponds to the molecular weight of the PET chain in g·mol^{-1}. The end-to-end distances were computed using the *gmx distance* tool built in GROMACS. The value of M = 2720.44 g·mol^{-1} was considered for a 14-monomer PET chain comprising one head-PET, 12 main-chain PET, and one tail-PET units.

To characterize how *Is*PETase approaches the PET surface, multiple metrics have been calculated throughout the adsorption simulation trajectories. These metrics include the contact area, number of contacts, and distance between specific atoms of the adsorbate/adsorbent. The contact area between *Is*PETase and the PET surfaces was determined considering the solvent-accessible surface areas of the isolated *Is*PETase ($SASA_{PETase}$), the PET surface ($SASA_{PT}$), and the *Is*PETase-PET complex ($SASA_{PETase-PET}$), which were gathered using the *gmx sasa* tool from GROMACS. The contact area was then calculated according to the following expression, as performed elsewhere:[25]

$$\text{Contact area} = \frac{\left((SASA_{PETase} + SASA_{PET}) - SASA_{PETase\text{-}PET}\right)}{2}$$

The number of contacts, defined as the number of non-hydrogen *Is*PETase atoms within 6 Å of the carbon atoms of the PET surface, was determined using the *gmx mindist* tool from GROMACS. The same tool was used to determine the minimum distance between any atoms of *Is*PETase and PET. Whenever necessary, the *gmx distance* tool from GROMACS was used to compute the distance between pairs of positions (*e.g.*, between atoms, between the center of mass of two groups of atoms) as a function of simulation time. The *gmx gangle* tool from GROMACS was used to calculate the orientation angle of the adsorbed *Is*PETase on the PET surfaces. This is defined as the angle between the plane of the PET surface (*i.e.*, the direction of the Z axis, after aligning the PET chains in the direction of the X axis using GROMACS *gmx editconf* tool) and the unit vector drawn from the *Is*PETase center of mass toward the catalytic Ser160 residue.

1.6. Computational resources

The vast majority of the simulations were conducted on the JURECA Data Centric (JURECA-DC) supercomputer at Jülich Supercomputing Centre.[26] Each node comprises two sockets, each housing a 64-core AMD EPYC Rome 7742 processor @ 2.25 GHz, equipped with 512 GB (16 × 32 GB) of DDR4 RAM. An InfiniBand HDR100/HDR network is used to connect computing nodes.

2. Supporting Figures

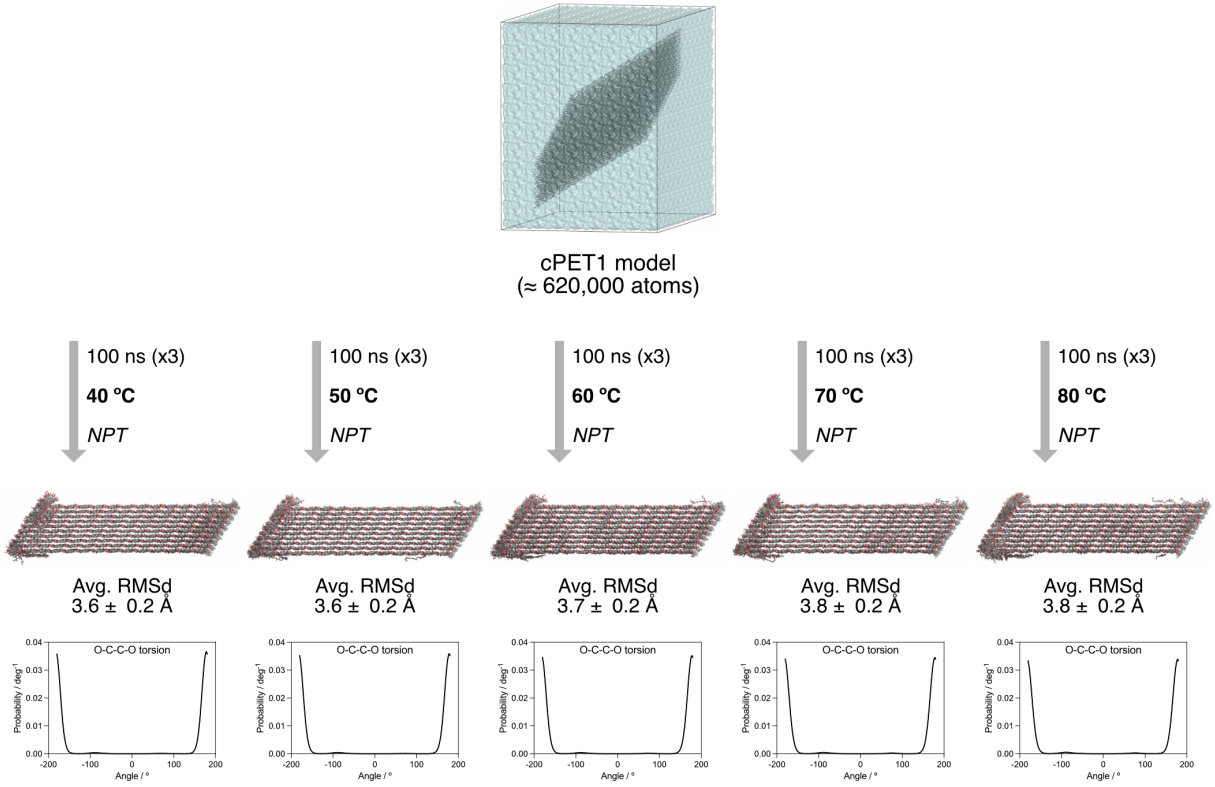

Fig. S1. Assessing the stability of the cPET1 model at a wide range of temperatures. cPET1 retained its crystalline arrangement at all tested temperatures (40-80 ºC), as reflected by the identical 3D structures and by the similar distribution of the torsion angle O-C-C-O in the EG units of all PET monomers.

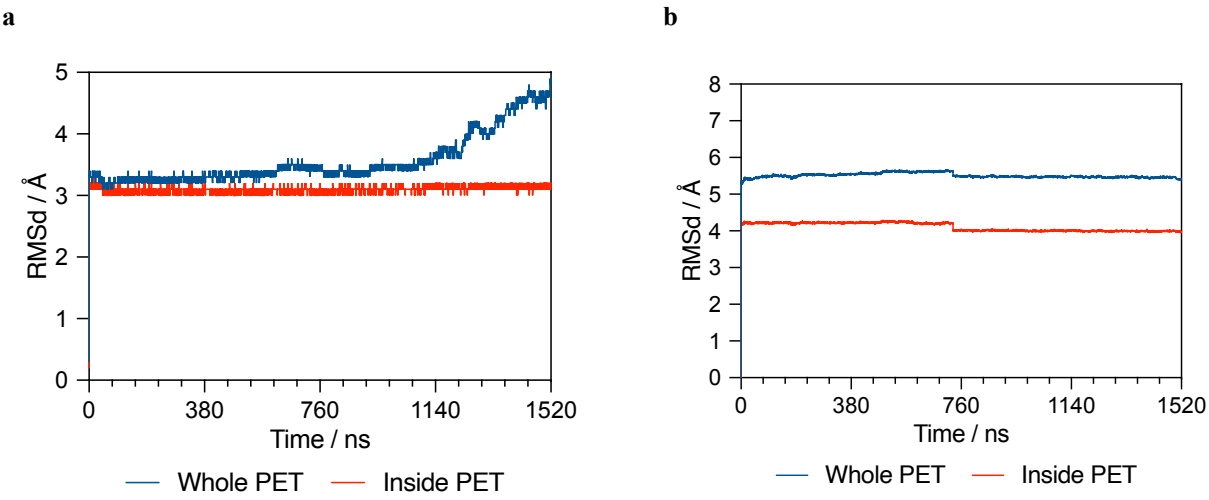

Fig. S2. RMSd for the cPET1 (simulated at 80 ºC for 1.52 µs) and cPET2 (simulated at 30 ºC for 1.52 µs) models as a function of time. The blue line corresponds to the RMSd values calculated for the entire cPET1 or cPET2 polymers. The red line concerns the RMSd values of cPET1 or cPET2 calculated after excluding the top and bottom layers of PET and the terminal monomers of each chain.

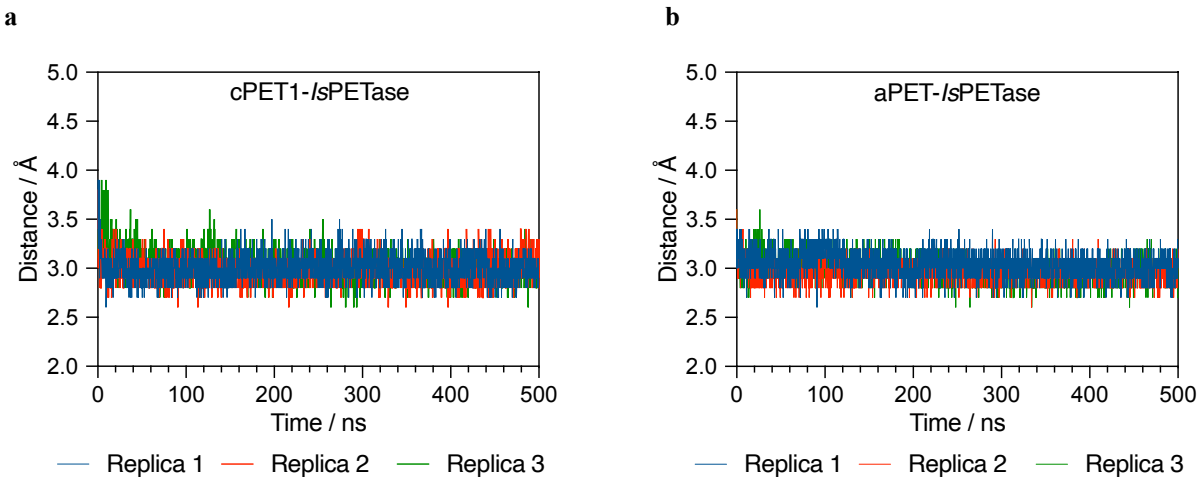

Fig. S3. Minimum distance between non-hydrogen atoms of *Is*PETase and the carbon atoms of either cPET1 (a) or aPET (b) polymers as a function of time. The calculated metric is presented for each 500 ns replica: Replica 1 in blue, Replica 2 in red, and Replica 3 in green.

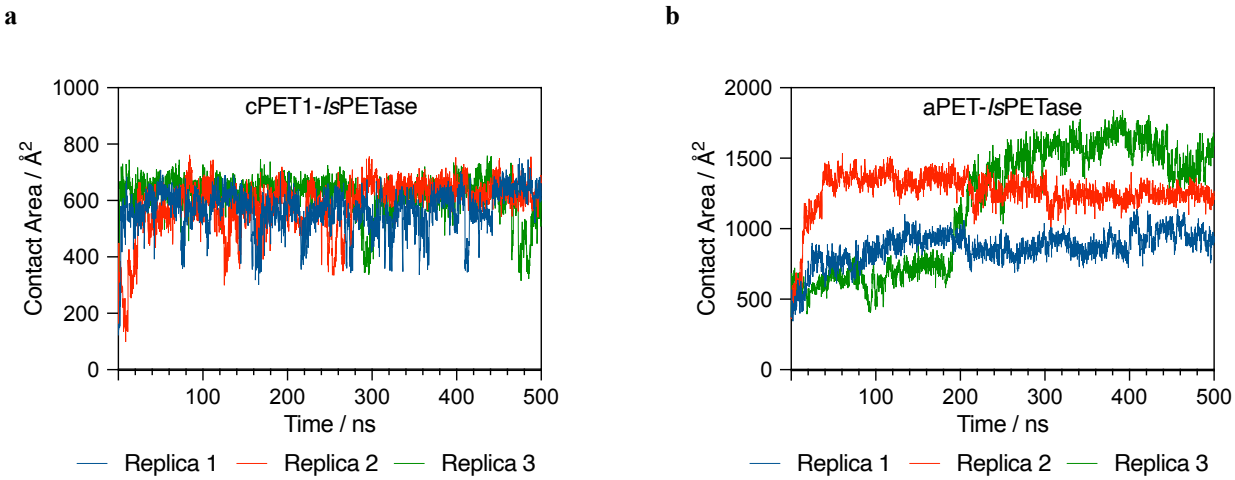

Fig. S4. Contact area between the *Is*PETase enzyme and either cPET1 (a) or aPET (b) surfaces as a function of time. The calculated metric is presented for each 500 ns replica: Replica 1 in blue, Replica 2 in red, and Replica 3 in green.

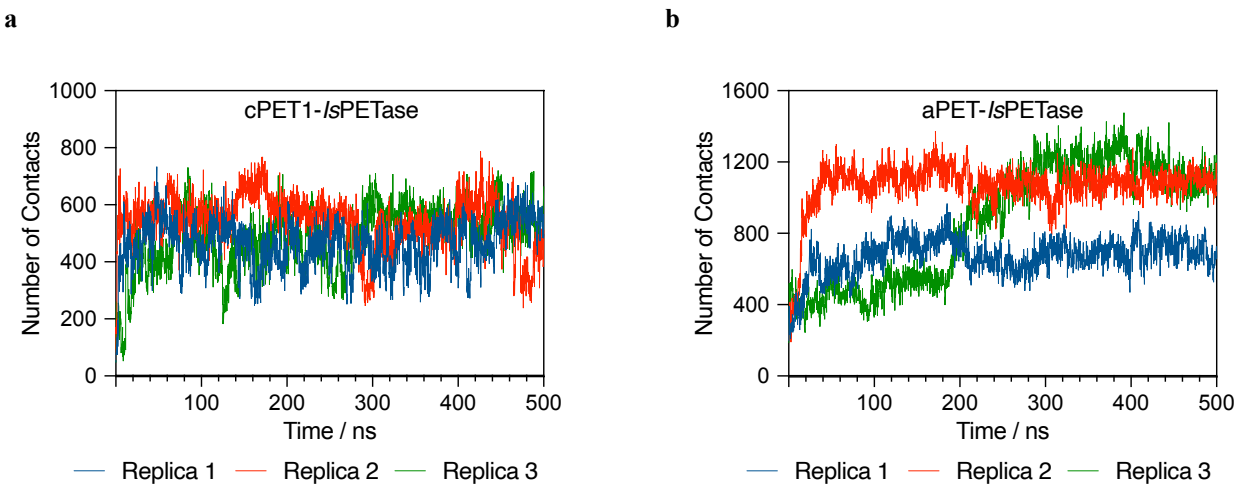

Fig. S5. Number of contacts (*i.e.*, number of non-hydrogen *Is*PETase atoms within 6 Å of the carbon atoms of the PET surface) established between *Is*PETase and either cPET1 (a) or aPET (b) surfaces as a function of time. The calculated metric is presented for each 500 ns replica: Replica 1 in blue, Replica 2 in red, and Replica 3 in green.

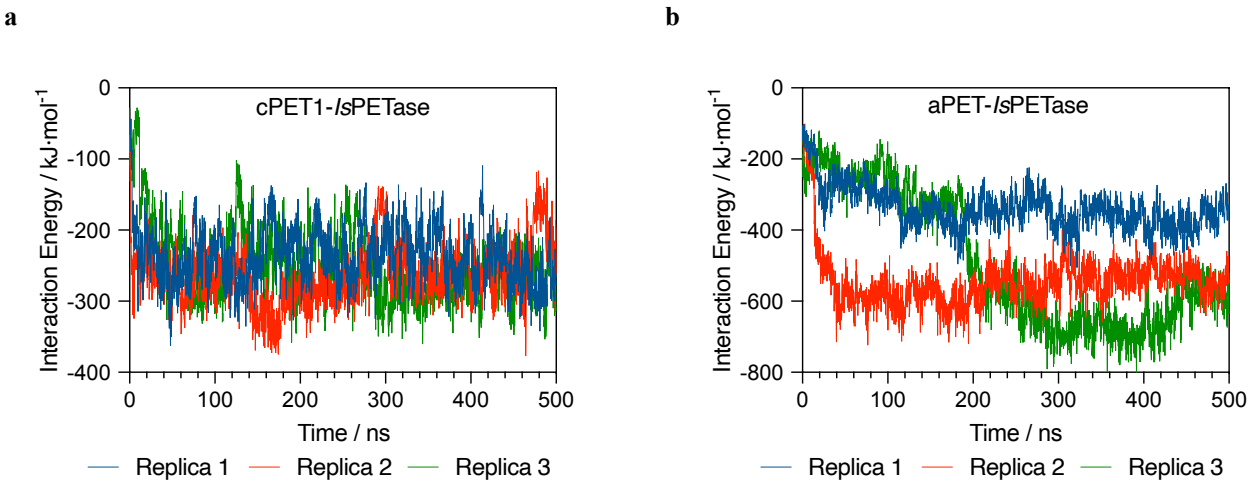

Fig. S6. Interaction energy between the *Is*PETase enzyme and the cPET1 (a) or aPET (b) surfaces as a function of time. The calculated metric is presented for each 500 ns replica: Replica 1 in blue, Replica 2 in red, and Replica 3 in green.

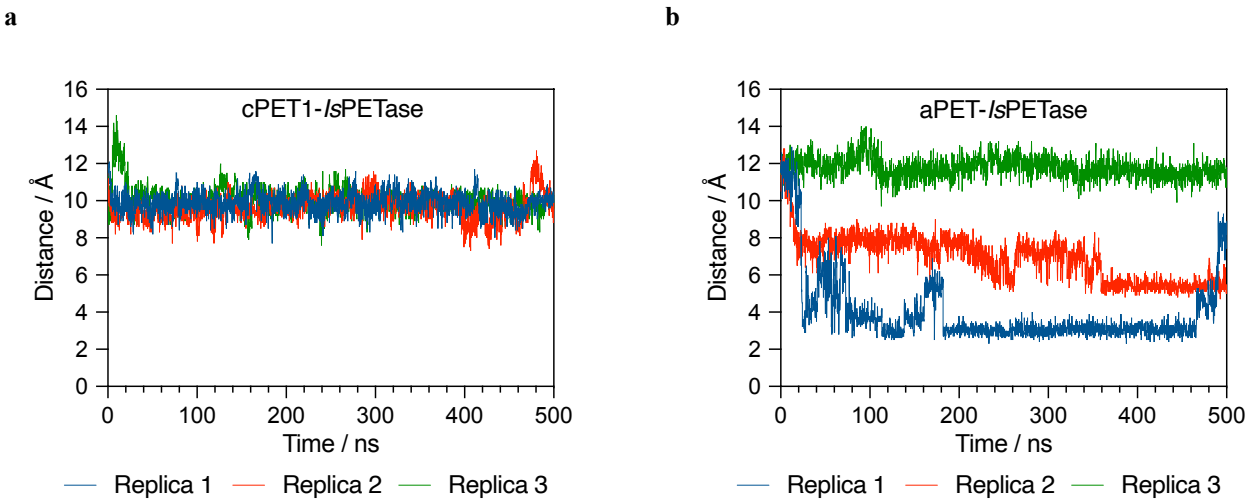

Fig. S7. Minimum distance between the center of mass of *Is*PETase's Ser160 and the ester carbon atoms of either cPET1 (a) or aPET (b) surfaces as a function of time. The calculated metric is presented for each 500 ns replica: Replica 1 in blue, Replica 2 in red, and Replica 3 in green.

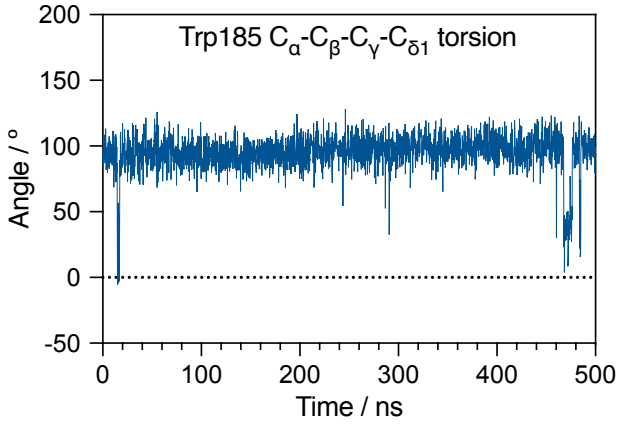

Fig. S8. The torsional angle between C_α-C_β-C_γ-$C_{\delta 1}$ atoms of W185 determined for the Replica 1 of the *Is*PETase adsorption on aPET as a function of time.

3. Supporting Tables

Table S1. Average RMSd values ± standard deviation of the cPET1 and cPET2 polymers, calculated for each MD simulation ran with these models.

Model	Temperature / ºC	Simulation	RMSd / Å
cPET1	30	**Rep1 - 100 ns**	3.6 ± 0.2
		Rep2 - 100 ns	3.5 ± 0.2
		Rep3 - 100 ns	3.7 ± 0.2
		Average (3 x 100 ns)	3.6 ± 0.2
	40	**Rep1 - 100 ns**	3.6 ± 0.2
		Rep2 - 100 ns	3.6 ± 0.2
		Rep3 - 100 ns	3.7 ± 0.2
		Average (3 x 100 ns)	3.6 ± 0.2
	50	**Rep1 - 100 ns**	3.6 ± 0.2
		Rep2 - 100 ns	3.6 ± 0.2
		Rep3 - 100 ns	3.6 ± 0.2
		Average (3 x 100 ns)	3.6 ± 0.2
	60	**Rep1 - 100 ns**	3.7 ± 0.2
		Rep2 - 100 ns	3.7 ± 0.2
		Rep3 - 100 ns	3.7 ± 0.2
		Average (3 x 100 ns)	3.7 ± 0.2
	70	**Rep1 - 100 ns**	3.9 ± 0.2
		Rep2 - 100 ns	3.7 ± 0.2
		Rep3 - 100 ns	3.7 ± 0.2
		Average (3 x 100 ns)	3.8 ± 0.2
	80	**Rep1 - 100 ns**	3.9 ± 0.2
		Rep2 - 100 ns	3.9 ± 0.2
		Rep3 - 100 ns	3.8 ± 0.2
		Average (3 x 100 ns)	3.8 ± 0.2
		1.52 µs	3.6 ± 0.4
cPET2	30	**Rep1 - 100 ns**	3.4 ± 0.2
		Rep2 - 100 ns	3.4 ± 0.2
		Rep3 - 100 ns	3.8 ± 0.2
		Average (3 x 100 ns)	3.5 ± 0.2
		1.52 µs	5.5 ± 0.1

Table S2. *Trans*/*gauche* ratio and *trans* content values of the cPET1 and cPET2 polymers, calculated for each MD simulation performed with these models. Whenever applicable, the values are presented as average ± standard deviation.

Model	Temperature / ºC	Simulation	*Trans*/*gauche* ratio	*Trans* content (%)
cPET1	30	**Rep1 - 100 ns**	137.82	64.47
		Rep2 - 100 ns	142.16	64.64
		Rep3 - 100 ns	169.85	64.71
		Average (3 x 100 ns)	149.94 ± 17.38	64.61 ± 0.12
	40	**Rep1 - 100 ns**	108.55	63.64
		Rep2 - 100 ns	128.20	63.82
		Rep3 - 100 ns	98.56	63.56
		Average (3 x 100 ns)	111.77 ± 15.08	63.67 ± 0.13
	50	**Rep1 - 100 ns**	106.60	62.77
		Rep2 - 100 ns	100.30	62.76
		Rep3 - 100 ns	111.48	62.74
		Average (3 x 100 ns)	106.13 ± 5.60	62.76 ± 0.02
	60	**Rep1 - 100 ns**	84.67	61.81
		Rep2 - 100 ns	100.57	61.85
		Rep3 - 100 ns	85.52	61.90
		Average (3 x 100 ns)	90.25 ± 8.94	61.85 ± 0.05
	70	**Rep1 - 100 ns**	74.01	61.02
		Rep2 - 100 ns	70.26	60.80
		Rep3 - 100 ns	70.58	60.7
		Average (3 x 100 ns)	71.62 ± 2.08	60.85 ± 0.15
	80	**Rep1 - 100 ns**	69.52	59.80
		Rep2 - 100 ns	59.32	59.72
		Rep3 - 100 ns	62.61	59.96
		Average (3 x 100 ns)	63.82 ± 5.21	59.83 ± 0.12
		1.52 µs	34.32	58.54
cPET2	30	**Rep1 - 100 ns**	80.34	62.01
		Rep2 - 100 ns	74.65	61.88
		Rep3 - 100 ns	65.84	60.99
		Average (3 x 100 ns)	73.61 ± 7.30	61.63 ± 0.56
		1.52 µs	49.51	60.64

Table S3. *Trans*/*gauche* ratio and *trans* content values of the cPET2 polymer, calculated for each MD stage conducted to transform the crystalline polymer into a completely amorphous one.

Temperature / ºC	*Trans*/*gauche* ratio	*Trans*/*gauche* ratio (%)	*Trans* content (%)
0	3441.86	344185.81	100.00
30	62.288	6228.81	60.84
55	47.198	4719.82	57.97
80	45.708	4570.77	57.50
105	42.396	4239.55	55.84
130	35.013	3501.28	52.34
155	30.878	3087.80	51.18
180	27.290	2729.01	49.28
205	16.590	1659.02	46.64
230	11.521	1152.14	45.34
255	6.683	668.33	38.95
280	3.332	333.17	32.53
305	1.422	142.21	21.48
330	0.076	7.55	2.10

Table S4. *Trans*/*gauche* ratio and *trans* content values of the aPET models, calculated for each MD simulation performed with these models. Whenever applicable, the values are presented as average ± standard deviation.

Model	Simulation	*Trans*/*gauche* ratio	*Trans*/*gauche* ratio (%)	*Trans* content (%)
aPET + Solvent	**Rep1 - 100 ns**	0.055	5.47	1.75
	Rep2 - 100 ns	0.054	5.41	1.75
	Rep3 - 100 ns	0.055	5.53	1.78
	Average (3 x 100 ns)	0.055 ± 0.001	5.47 ± 0.06	1.76 ± 0.02
	500 ns	0.051	5.10	1.69
aPET in Vacuum	**Rep1 - 100 ns**	0.072	7.17	2.12
	Rep2 - 100 ns	0.077	7.69	2.24
	Rep3 - 100 ns	0.073	7.25	2.13
	Average (3 x 100 ns)	0.074 ± 0.003	7.37 ± 0.28	2.16 ± 0.07
	500 ns	0.069	6.92	2.05

Table S5. Characteristic ratio values of the aPET models, calculated for each MD simulation performed with these models. The values are presented as average ± standard deviation.

Model	Simulation	C. Ratio x 10^{-3} / $nm^2 \cdot mol \cdot g^{-1}$
aPET + Solvent	**Rep1 - 100 ns**	6.35 ± 0.02
	Rep2 - 100 ns	6.35 ± 0.01
	Rep3 - 100 ns	6.37 ± 0.01
	Average (3 x 100 ns)	6.36 ± 0.02
	500 ns	6.40 ± 0.02
aPET in Vacuum	**Rep1 - 100 ns**	6.54 ± 0.03
	Rep2 - 100 ns	6.56 ± 0.03
	Rep3 - 100 ns	6.48 ± 0.04
	Average (3 x 100 ns)	6.52 ± 0.05
	500 ns	6.49 ± 0.07

Table S6. *Trans*/*gauche* ratio and *trans* content values of the cPET1 and aPET polymers that comprise the cPET1-*Is*PETase and aPET-*Is*PETase systems, respectively, calculated for each MD simulation performed with these systems. Whenever applicable, the values are presented as average ± standard deviation.

System	Simulation	*Trans*/*gauche* ratio	*Trans* content (%)
cPET1-*Is*PETase	**Rep1 - 500 ns**	78.07	64.21
	Rep2 - 500 ns	85.73	64.32
	Rep3 - 500 ns	79.59	64.38
	Average (3 x 500 ns)	81.13 ± 4.05	64.30 ± 0.09
aPET-*Is*PETase	**Rep1 - 500 ns**	0.050	1.64
	Rep2 - 500 ns	0.052	1.72
	Rep3 - 500 ns	0.054	1.75
	Average (3 x 500 ns)	0.052 ± 0.002	1.70 ± 0.06

Table S7. Average characteristic ratio values of the aPET polymer of the aPET-*Is*PETase system, calculated for each MD simulation performed with this system. The values are presented as average ± standard deviation.

System	Simulation	C. Ratio x 10^{-3} / $nm^2 \cdot mol \cdot g^{-1}$
aPET-*Is*PETase	**Rep1 - 500 ns**	6.45 ± 0.04
	Rep2 - 500 ns	6.46 ± 0.05
	Rep3 - 500 ns	6.42 ± 0.03
	Average (3 x 500 ns)	6.44 ± 0.05

Table S8. Average values of the orientation angle of the adsorbed *Is*PETase on the cPET1 and aPET surfaces. The values are presented as average ± standard deviation.

System	Simulation	Orientation Angle / º
cPET1-*Is*PETase	**Rep1 - 500 ns**	103.7 ± 2.8
	Rep2 - 500 ns	103.5 ± 2.7
	Rep3 - 500 ns	101.6 ± 5.2
	Average (3 x 500 ns)	102.9 ± 3.9
aPET-*Is*PETase	**Rep1 - 500 ns**	108.7 ± 11.0
	Rep2 - 500 ns	107.7 ± 3.5
	Rep3 - 500 ns	46.6 ± 13.8
	Average (3 x 500 ns)	87.7 ± 30.8

Table S9. Average backbone and all-atom RMSd values ± standard deviation concerning the *Is*PETase enzyme, calculated for each MD simulation where this enzyme adsorbed in a PET surface.

	System	Simulation	RMSd / Å
Backbone	**cPET1-*Is*PETase**	**Rep1 - 500 ns**	1.1 ± 0.1
		Rep2 - 500 ns	1.1 ± 0.2
		Rep3 - 500 ns	1.1 ± 0.2
		Average (3 x 500 ns)	1.1 ± 0.2
	aPET-*Is*PETase	**Rep1 - 500 ns**	1.1 ± 0.2
		Rep2 - 500 ns	1.3 ± 0.2
		Rep3 - 500 ns	1.0 ± 0.2
		Average (3 x 500 ns)	1.1 ± 0.2
All-atom	**cPET1-*Is*PETase**	**Rep1 - 500 ns**	1.6 ± 0.1
		Rep2 - 500 ns	1.7 ± 0.2
		Rep3 - 500 ns	1.7 ± 0.2
		Average (3 x 500 ns)	1.7 ± 0.2
	aPET-*Is*PETase	**Rep1 - 500 ns**	1.6 ± 0.2
		Rep2 - 500 ns	1.9 ± 0.1
		Rep3 - 500 ns	1.6 ± 0.2
		Average (3 x 500 ns)	1.7 ± 0.2

Table S10. Contact area and number of contacts between *Is*PETase and either the cPET1 or aPET polymers, calculated for each MD simulation where this enzyme adsorbed in a PET surface. The values are presented as average ± standard deviation.

System	Simulation	Contact Area / Å^2	Number of contacts[#]
cPET1-*Is*PETase	**Rep1 - 500 ns**	564.7 ± 75.7	464 ± 84
	Rep2 - 500 ns	585.8 ± 96.1	544 ± 91
	Rep3 - 500 ns	617.8 ± 69.8	490 ± 110
	Average (3 x 500 ns)	589.5 ± 84.2	499 ± 101
aPET-*Is*PETase	**Rep1 - 500 ns**	867.3 ± 115.0	671 ± 105
	Rep2 - 500 ns	1258.8 ± 141.9	1064 ± 138
	Rep3 - 500 ns	1174.4 ± 431.8	867 ± 332
	Average (3 x 500 ns)	1100.2 ± 318.7	868 ± 269

[#]A contact is considered to exist if the distance between non-hydrogen *Is*PETase atoms and carbon atoms of the PET surface is less than 6 Å

Table S11. Minimum distance between the center of mass of *Is*PETase's Ser160 and the ester carbon atoms of either cPET1 or aPET surfaces, **calculated for each MD simulation that addressed the adsorption of *Is*PETase on PET.** The values are presented as average ± standard deviation.

System	Simulation	Distance / Å
cPET1-*Is*PETase	**Rep1 - 500 ns**	9.90 ± 0.57
	Rep2 - 500 ns	9.68 ± 0.66
	Rep3 - 500 ns	10.08 ± 0.68
	Average (3 x 500 ns)	9.89 ± 0.66
aPET-*Is*PETase	**Rep1 - 500 ns**	3.99 ± 1.94
	Rep2 - 500 ns	6.93 ± 1.28
	Rep3 - 500 ns	11.78 ± 0.56
	Average (3 x 500 ns)	7.57 ± 3.50

Table S12. Frequency of MD frames that display catalytically relevant distances (*i.e.*, distances between the catalytic triad residues Ser160/His237/Asp206) below the 3.5 Å threshold. Whenever applicable, the values are presented as average ± standard deviation.

System	Simulation	Frequency / %
cPET1-*Is*PETase	**Rep1 - 500 ns**	9.9
	Rep2 - 500 ns	10.5
	Rep3 - 500 ns	11.6
	Average (3 x 500 ns)	10.6 ± 0.9
aPET-*Is*PETase	**Rep1 - 500 ns**	44.5
	Rep2 - 500 ns	35.9
	Rep3 - 500 ns	24.0
	Average (3 x 500 ns)	34.8 ± 10.3

Table S13. PET models that were developed in this work.

Model	No. of PET monomers	PET polymer' dimensions (W x L x H)	Solvent	No. of atoms of the system
cPET1	3640	≈ 150 x 155 x 45 Å	Yes	≈ 620,000
cPET2	7280	≈ 150 x 155 x 90 Å	No	≈ 164,000
aPET + Solvent	7280	≈ 130 x 300 x 85 Å	Yes	≈ 1,407,000
aPET in Vacuum	7280	≈ 130 x 300 x 85 Å	No	≈ 164,000

Table S14. MD stages concerning the simulations of the cPET models.

Model	Stage	Ensemble	Temp. / ºC	Positional restraints	Simulation time / ns
cPET1	Heating	*NVT*[#]	30-80[*]	PET atoms	0.5
	Equilibration	*NPT*[#†]	30-80[*]	PET atoms	0.5
	Production	*NPT*[#¶]	30-80[*]	-	100 / 1520[≠]
cPET2	Heating	*NVT*[#]	30	PET atoms	0.5
	Equilibration	*NVT*[#]	30	PET atoms	0.5
	Production	*NVT*[#]	30	-	100 / 1520[§]

[#] The V-rescale thermostat[27] was used to linearly heat the system to the corresponding temperature.

[*] The simulations were conducted at six different temperature stages. ranging from 30 to 80 ºC (30 ºC. 40 ºC. 50 ºC. 60 ºC. 70 ºC and 80 ºC).

[†] The pressure was kept constant at approximately 1.0 bar using the Berendsen barostat.[28]

[¶] The pressure was kept constant at approximately 1.0 bar using the the Parrinello-Rahman barostat.[29]

[≠] A single simulation of 1.52 μs was performed at 80 ºC to follow the overall stability of the cPET1 system in a very long simulation.

[§] A single simulation of 1.52 μs was performed to follow the behavior of the cPET2 system over a longer period.

Table S15. MD stages of the equilibration cycle used to generate the relaxed aPET model.

Equilibration stage	Ensemble	Temperature* / ºC	Pressure≠ / bar	Simulation time / ps
1	*NVT*	327	-	50
2	*NVT*	27	-	50
3	*NPT*	27	1000	50
4	*NVT*	327	-	50
5	*NVT*	27	-	100
6	*NPT*	27	30000	50
7	*NVT*	327	-	50
8	*NVT*	27	-	100
9	*NPT*	27	5000	50
10	*NVT*	327	-	50
11	*NVT*	27	-	100
12	*NPT*	27	1	10000

* Temperature was maintained constant using the V-rescale thermostat.

≠ The Berendsen barostat was used to control the pressure in *NPT* simulations.

Table S16. MD stages conducted to determine the T_g of the aPET model.

Cycle	Stage	Ensemble	Temp. / ºC	Simulation time / ns
1	Heating	*NVT*#	327	0.05
	Production	*NPT*#†	327	10
2-15	Cooling	*NVT*#	Cooling rate of 5 ºC / ns	5
	Equilibration	*NPT*#†	30	10
	Production	*NPT*#†	30	30

The V-rescale thermostat[27] was used to linearly heat the system to the corresponding temperature.

† The pressure was kept constant at approximately 1.0 bar using the Berendsen barostat.

Table S17. MD stages concerning the simulations of the aPET models.

Model	Stage	Ensemble	Temp. / ºC	Positional restraints	Simulation time / ns
aPET + Solvent	Heating	*NVT*#	30	PET atoms	0.5
	Equilibration	*NPT*#†	30	PET atoms	0.5
	Production	*NPT*#¶	30	-	100 / 500§
aPET2 in Vacuum	Heating	*NVT*#	30	PET atoms	0.5
	Equilibration	*NVT*#	30	PET atoms	0.5
	Production	*NVT*#	30	-	100 / 500§

The V-rescale thermostat was used to linearly heat the system and to control its temperature.

† The pressure was kept constant at approximately 1.0 bar using the Berendsen barostat.

¶ The pressure was kept constant at approximately 1.0 bar using the the Parrinello-Rahman barostat.

§ A single simulation of 500 ns was performed to follow the behavior of the aPET models over a longer period.

4. Supporting References

1. D. Case, I. Ben-Shalom, S. R. Brozell, D. S. Cerutti, T. Cheatham, V. W. D. Cruzeiro, T. Darden, R. Duke, D. Ghoreishi, M. Gilson, H. Gohlke, A. Götz, D. Greene, R. Harris, N. Homeyer, Y. Huang, S. Izadi, A. Kovalenko, T. Kurtzman and P. A. Kollman, *Amber 2018*, University of California, San Francisco, 2018.
2. M. D. Hanwell, D. E. Curtis, D. C. Lonie, T. Vandermeersch, E. Zurek and G. R. Hutchison, *J. Cheminform.*, 2012, **4**, 17.
3. R. D. P. Daubeny, C. W. Bunn, C. J. Brown and W. L. Bragg, *Proceedings of the Royal Society of London. Series A. Mathematical and Physical Sciences*, 1954, **226**, 531-542.
4. J. C. Lightfoot, A. Buchard, B. Castro-Dominguez and S. C. Parker, *Macromolecules*, 2022, **55**, 498-510.
5. M. J. T. Frisch, G. W.; Schlegel, H. B.; Scuseria, G. E.; Robb, M. A.; Cheeseman, J. R.; Scalmani, G.; Barone, V.; Petersson, G. A.; Nakatsuji, H.; Li, X.; Caricato, M.; Marenich, A.; Bloino, J.; Janesko, B. G.; Gomperts, R.; Mennucci, B.; Hratchian, H. P.; Ortiz, J. V.; Izmaylov, A. F.; Sonnenberg, J. L.; Williams-Young, D.; Ding, F.; Lipparini, F.; Egidi, F.; Goings, J.; Peng, B.; Petrone, A.; Henderson, T.; Ranasinghe, D.; Zakrzewski, V. G.; Gao, J.; Rega, N.; Zheng, G.; Liang, W.; Hada, M.; Ehara, M.; Toyota, K.; Fukuda, R.; Hasegawa, J.; Ishida, M.; Nakajima, T.; Honda, Y.; Kitao, O.; Nakai, H.; Vreven, T.; Throssell, K.; Montgomery, Jr., J. A.; Peralta, J. E.; Ogliaro, F.; Bearpark, M.; Heyd, J. J. ; Brothers, E.; Kudin, K. N.; Staroverov, V. N.; Keith, T.; Kobayashi, R.; Normand, J.; Raghavachari, K.; Rendell, A.; Burant, J. C.; Iyengar, S. S.; Tomasi, J.; Cossi, M.; Millam, J. M.; Klene, M.; Adamo, C.; Cammi, R.; Ochterski, J. W.; Martin, R. L.; Morokuma, K.; Farkas, O.; Foresman, J. B.; Fox, D. J., *Gaussian, Inc.: Wallingford, CT*, 2009.
6. W. D. C. Cornell, P.; Bayly, C. I.; Gould, I. R.; Merz, K. M.; Ferguson, D. M.; Spellmeyer, D. C.; Fox, T.; Caldwell, J. W.; Kollman, P. A., *J. Am. Chem. Soc.*, 1996, **118 (9)**, 2309-2309.
7. W. L. Jorgensen, J. Chandrasekhar, J. D. Madura, R. W. Impey and M. L. Klein, *J. Chem. Phys.*, 1983, **79**, 926-935.
8. M. J. Abraham, T. Murtola, R. Schulz, S. Páll, J. C. Smith, B. Hess and E. Lindahl, *SoftwareX*, 2015, **1-2**, 19-25.
9. D. Van Der Spoel, E. Lindahl, B. Hess, G. Groenhof, A. E. Mark and H. J. Berendsen, *J. Comput. Chem.*, 2005, **26**, 1701-1718.
10. M. R. Shirts, C. Klein, J. M. Swails, J. Yin, M. K. Gilson, D. L. Mobley, D. A. Case and E. D. Zhong, *J. Comput. Aided Mol. Des.*, 2017, **31**, 147-161.

11. U. Essmann, L. Perera, M. L. Berkowitz, T. Darden, H. Lee and L. G. Pedersen, *The Journal of Chemical Physics*, 1995, **103**, 8577-8593.
12. B. Hess, H. Bekker, H. J. C. Berendsen and J. G. E. M. Fraaije, *J. Comput. Chem.*, 1997, **18**, 1463-1472.
13. V. Tournier, S. Duquesne, F. Guillamot, H. Cramail, D. Taton, A. Marty and I. Andre, *Chem Rev*, 2023, DOI: 10.1021/acs.chemrev.2c00644.
14. R. Wei, D. Breite, C. Song, D. Grasing, T. Ploss, P. Hille, R. Schwerdtfeger, J. Matysik, A. Schulze and W. Zimmermann, *Adv Sci (Weinh)*, 2019, **6**, 1900491.
15. S. Yoshida, K. Hiraga, T. Takehana, I. Taniguchi, H. Yamaji, Y. Maeda, K. Toyohara, K. Miyamoto, Y. Kimura and K. Oda, *Science*, 2016, **351**, 1196-1199.
16. D. Hofmann, L. Fritz, J. Ulbrich, C. Schepers and M. Böhning, *Macromol. Theory Simul.*, 2000, **9**, 293-327.
17. N. C. Karayiannis, V. G. Mavrantzas and D. N. Theodorou, *Macromolecules*, 2004, **37**, 2978-2995.
18. H. P. Austin, M. D. Allen, B. S. Donohoe, N. A. Rorrer, F. L. Kearns, R. L. Silveira, B. C. Pollard, G. Dominick, R. Duman, K. El Omari, V. Mykhaylyk, A. Wagner, W. E. Michener, A. Amore, M. S. Skaf, M. F. Crowley, A. W. Thorne, C. W. Johnson, H. L. Woodcock, J. E. McGeehan and G. T. Beckham, *Proc. Natl. Acad. Sci. U. S. A.*, 2018, **115**, E4350-E4357.
19. M. H. M. Olsson, C. R. Søndergaard, M. Rostkowski and J. H. Jensen, *J. Chem. Theory Comput.*, 2011, **7**, 525-537.
20. Schrodinger, LLC, unpublished work.
21. J. A. Maier, C. Martinez, K. Kasavajhala, L. Wickstrom, K. E. Hauser and C. Simmerling, *J. Chem. Theory Comput.*, 2015, **11**, 3696-3713.
22. K. Schmidt-Rohr, W. Hu and N. Zumbulyadis, *Science*, 1998, **280**, 714-717.
23. H. Eslami and F. Müller-Plathe, *Macromolecules*, 2009, **42**, 8241-8250.
24. A. D. Williams and P. J. Flory, *Journal of Polymer Science Part A-2: Polymer Physics*, 1967, **5**, 417-424.
25. K. Balamurugan, E. R. A. Singam and V. Subramanian, *The Journal of Physical Chemistry C*, 2011, **115**, 8886-8892.
26. P. Thörnig, *Journal of large-scale research facilities JLSRF*, 2021, **7**, A182-A182.
27. G. Bussi, D. Donadio and M. Parrinello, *J. Chem. Phys.*, 2007, **126**, 014101.
28. H. J. C. Berendsen, J. P. M. Postma, W. F. van Gunsteren, A. DiNola and J. R. Haak, *The Journal of Chemical Physics*, 1984, **81**, 3684-3690.
29. M. Parrinello and A. Rahman, *J. Appl. Phys.*, 1981, **52**, 7182-7190.